THE JOURNAL OF PHYSICAL CHEMISTRY B

Article

pubs.acs.org/JPCB

Femtosecond Dynamics of Excitons and Hole-Polarons in Composite P3HT/PCBM Nanoparticles

Scott N. Clafton, David M. Huang, William R. Massey, and Tak W. Kee*

School of Chemistry & Physics, The University of Adelaide, Adelaide, South Australia 5005, Australia

Supporting Information

ABSTRACT: The dynamics of charge separation in aqueous suspensions of regioregular P3HT nanoparticles containing PCBM were investigated for the first time using femtosecond transient absorption spectroscopy. This investigation is supported by the recently reported use of regioregular P3HT/PCBM nanoparticles as charge trapping and storage devices. In this study, the presence of excited-state and charge-separated species, including singlet excitons, polymer polarons and free charges, generated in rr-P3HT/PCBM nanoparticles was identified through visible pump and visible/near-infrared probe femtosecond transient absorption spectroscopy at a range of electron acceptor concentrations. The decrease of the singlet exciton lifetime by charge transfer to PCBM is well described by a one-dimensional diffusion model with a P3HT domain size of approximately 5 nm for 5−50 wt % PCBM. This model also indicates that bimolecular recombination is the dominant charge recombination mechanism at 20 wt % PCBM and above.

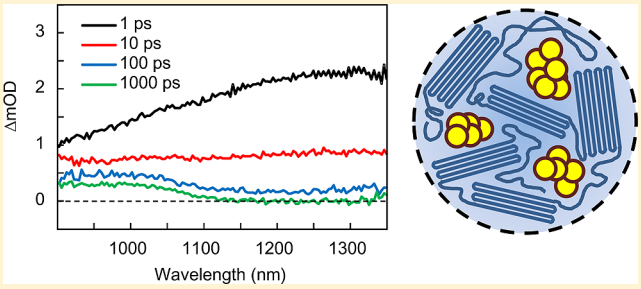

INTRODUCTION

Conjugated polymer nanoparticles have been the subject of increased attention in recent years for their applications in biological imaging and fluorescence sensing.[1−11] In particular, the impressive optical properties of conjugated polymers have been exploited by incorporating small sensing molecules into the nanoparticles that respond to environmental stimuli.[9−11] Recently, this method has been extended to the preparation of composite nanoparticles of regioregular poly(3-hexylthiophene-2,5-diyl) (rr-P3HT, Figure 1) containing the electron acceptor [6,6]-phenyl-C_{61} butyric acid methyl ester (PCBM) in aqueous suspensions.[12−15] Currently, there is significant interest in studying these composite nanoparticles because they are an intermediate system between bulk films and single molecules, with a limited number of molecules ranging from a few to a few tens of polymer chains. Composite nanoparticles offer functionality found in bulk materials but without significant heterogeneity in the system, thereby providing an opportunity to understand the links between functional materials and their molecular-level properties.[12−15]

The P3HT/PCBM blend is the most extensively studied donor/acceptor combination. Device efficiencies of around 4% are routinely reported for this blend and efficiencies as high as 6.5% have been measured.[16−18] Other desirable properties of organic donor/acceptor blends such as P3HT/PCBM include solution processability for fast and inexpensive device production using conventional printing techniques; however, this approach currently requires the use of hazardous organic solvents. Recently, there has been a trend toward using nonhazardous solvents including water for device preparation.

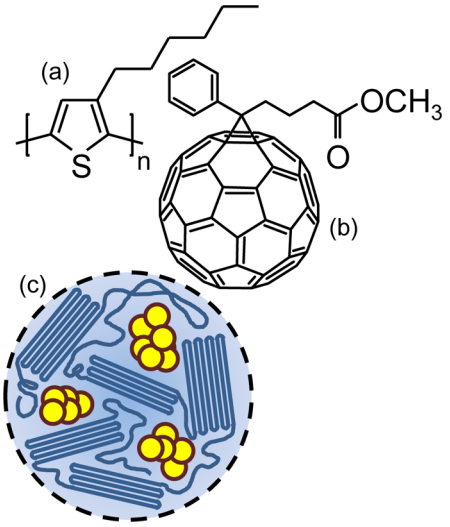

Figure 1. Chemical structures of (a) P3HT and (b) PCBM. (c) Illustration of a rr-P3HT nanoparticle with aggregated PCBM domains.

Most of the work thus far involves using water-soluble analogues of electron donor and acceptor materials.[19,20] An

Special Issue: Paul F. Barbara Memorial Issue

Received: September 6, 2012
Revised: February 4, 2013

   dx.doi.org/10.1021/jp308876z | J. Phys. Chem. B XXXX, XXX, XXX−XXX

alternative and more straightforward route to achieving solution processability with water is to use aqueous suspensions of existing photovoltaic materials. Therefore, understanding charge transfer and morphology in aqueous suspensions of these materials is important.

Although charge transfer has been demonstrated in aqueous suspensions of polymer/fullerene nanoparticles,[13,21,22] the ultrafast dynamics of excited-state and charge-separated species have not been investigated. Such studies have been performed extensively on thin-film devices covering a wide range of film properties that influence the efficiency of charge separation.[6,23−31] In particular, the effects of polymer morphology and the influence of P3HT/PCBM doping ratios have been key areas of study. Transient absorption spectra of highly ordered rr-P3HT and amorphous regiorandom P3HT (rra-P3HT) films both indicate formation of singlet excitons, polymer polarons, and charge-separated species,[24,32] albeit in varying spectral regions. Charge separation, which is of particular interest, is found to follow a two-step mechanism in both film morphologies.[24] Initially, polarons are generated through charge separation of excitons at the P3HT/PCBM interface. Subsequently, a relatively slow formation of polarons occurs as this process is limited by exciton migration. The rate of the second phase of polaron formation is slow in rr-P3HT because excitons must migrate through extended semicrystalline domains to undergo charge separation. Increasing electron acceptor concentration provides a greater interfacial area, which promotes charge separation immediately after excitation and enhances the probability for excitons to migrate to the PCBM interface successfully. Although these processes have been studied extensively in films, the excited-state species and their associated dynamics have not been identified for aqueous dispersions of P3HT/PCBM nanoparticles. In addition, a recent study on exciton−hole polaron interactions showed that P3HT/PCBM nanoparticles have the ability to store photogenerated charges due to the presence of deep electron traps.[14] The studies of the dynamics of P3HT excitons and other excited-state species are important for gaining an understanding of charge separation dynamics to offer insight into charge storage.

In this work, we investigate two key factors that influence the charge separation dynamics in aqueous suspensions of P3HT/PCBM nanoparticles, namely the regioregularity of P3HT and the concentration of PCBM. The steady-state fluorescence quenching studies offer insight into the relative charge transfer efficiency of rra-P3HT and rr-P3HT nanoparticles in which amorphous and semicrystalline morphologies, respectively, are present. Femtosecond transient absorption spectroscopy was then employed to identify excited-state and charge-separated species in the visible and near-infrared spectral regions. Formation and recombination dynamics of these species were also monitored to determine their dependence on electron acceptor concentration. By comparing the excited-state behavior of P3HT/PCBM nanoparticles with studies of thin films, the performance of nanoparticles in a device-like environment was evaluated. The average size of semicrystalline domains of rr-P3HT nanoparticles was then quantified using an exciton diffusion model for analyzing transient absorption signals of P3HT/PCBM films.[27] The evolution of the transient absorption signals showed excellent agreement with the exciton diffusion model for P3HT nanoparticles containing 5−50 wt % PCBM.

EXPERIMENTAL SECTION

Sample Preparation. Aqueous nanoparticle suspensions of rr-P3HT and rra-P3HT (Rieke Metals Inc.) doped with PCBM (Nano C) were prepared following the method established by Hu and Gesquiere.[13] The preparation of solely polymer nanoparticles required a solution of P3HT in freshly distilled tetrahydrofuran (THF, Scharlau) to be rapidly combined with water under vigorous agitation. Nanoparticles prepared using the same procedure were found to be stable for several weeks or longer due to a negative surface charge.[1,33] Water used in all experiments was purified using a 10 MΩ Millipore Milli-Q Reagent Water System. The remaining THF was then removed under reduced pressure to yield a fully aqueous suspension. Nanoparticle samples doped with 5, 10, 20, and 50 wt % PCBM were prepared by incorporating the required amount of electron acceptor into the precursor solution of P3HT in THF before the addition to water. It is important to note that wt % is the weight of PCBM per weight of PCBM and P3HT combined; i.e., 50 wt % corresponds to an equal weight of P3HT and PCBM. The weight of P3HT was maintained across all nanoparticle samples. The resulting suspensions were either concentrated to 8 ppm for steady-state optical characterization or 100 ppm for ultrafast transient absorption experiments.

Particle Size Characterization by Atomic Force Microscopy. The nanoparticle size distributions were characterized by atomic force microscopy using a NT-MDT Ntegra Solaris operating in semicontact mode. The tip used for these measurements was a NT-MDT NSG10, which had a 10 nm point and operates at 140−390 kHz. Dilute aqueous suspensions of conjugated polymer nanoparticles were deposited onto silicon wafers that had been cleaned in concentrated potassium hydroxide. Images were typically 3 × 3 μm^2 and taken at a rate of 0.5 Hz per line with a 256-line resolution. The vertical axis was calibrated by the NT-MDT TGS1 calibration set with a set height of 17 ± 1.2 nm. The size distributions for P3HT nanoparticles with 0, 5, and 50 wt % PCBM, which are shown in the Supporting Information, show good agreement with published data for these composite nanoparticles.[13] The estimated average diameters of rr-P3HT nanoparticles with 0, 5, and 50 wt % PCBM are 31, 33, and 52 nm, respectively, as shown in the Supporting Information.

Steady-State and Transient Absorption Spectroscopic Measurements. Steady-state absorption and fluorescence spectra of aqueous nanoparticle suspensions were recorded using Cary 300 Bio UV−vis (Varian) and Cary Eclipse fluorescence spectrophotometers, respectively. The excitation wavelength for all fluorescence data was 490 nm. The excitation and emission slit widths were 10 and 5 nm, respectively.

The laser system for the pump−probe femtosecond transient absorption experiments included a Ti:sapphire mode-locked oscillator (Spectra-Physics, Tsunami), which seeded a Ti:sapphire regenerative amplifier (Spectra-Physics, Spitfire Pro XP). A portion of the amplifier output, which was centered at 800 nm with a repetition rate of 1 kHz and pulse duration of 100 fs, was used to generate the 500 nm pump beam using a traveling wave optical parametric amplifier (Light Conversion, TOPAS-C). The visible or near-infrared probe light was derived from a white light continuum generated using a 2 or 13 mm sapphire plate, respectively, with another portion of the fundamental. The pump was mechanically chopped at 500 Hz and then focused onto the sample with a spot size of 890 μm and pulse energy of 50 nJ. The pump pulse energy level used is consistent

dx.doi.org/10.1021/jp308876z | J. Phys. Chem. B XXXX, XXX, XXX−XXX

with that in previous studies.[27,32] Minimal pump pulse energy was used in all experiments to reduce the probability of exciton−exciton annihilation and the associated influence on recombination dynamics. Meanwhile, the probe was passed through a delay stage prior to white light continuum generation. A beam splitter was used to divide the white light continuum into the sample and reference beams. The spot sizes at the sample position were 275 and 145 μm for the visible and near-infrared probe, respectively. The sample and reference beams were then directed into complementary CCD or metal-oxide semiconductor array detectors for detection in the visible or near-infrared regions, respectively. In all experiments the pump polarization was oriented at 54.7° relative to the probe polarization.

RESULTS AND DISCUSSION

Steady-State Absorption and Fluorescence Spectra. The absorption spectra of rr-P3HT nanoparticles doped with 0−50 wt % PCBM are shown in Figure 2a. These spectra

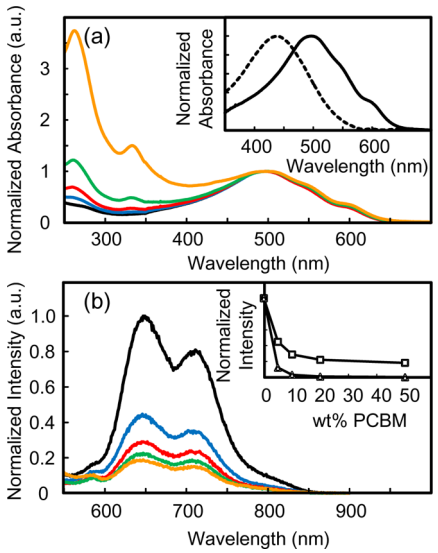

Figure 2. (a) Steady-state absorption spectra of rr-P3HT nanoparticles doped with 0 (black), 5 (blue), 10 (red), 20 (green), and 50 (orange) wt % PCBM. The inset shows the absorption spectrum of undoped rr-P3HT nanoparticles (solid) compared with rra-P3HT (dashed). (b) Fluorescence spectra of rr-P3HT nanoparticles doped with 0 (black), 5 (blue), 10 (red), 20 (green), and 50 (orange) wt % PCBM. The inset shows the normalized intensity at the fluorescence maximum of rr-P3HT (squares) and rra-P3HT (triangles).

consist of three major bands, which include two UV absorption bands at 260 and 340 nm due to PCBM and the visible absorption at 500 nm due to the $\pi-\pi^*$ transition of the polymer. It is well-known that rr-P3HT forms aggregates readily with a high degree of order, which is evidenced by the vibronic structure present on the red side of the rr-P3HT nanoparticle absorption spectrum, as shown by the solid curve in the Figure 2a inset.[34] To better understand how the formation of semicrystalline domains influences the structure within P3HT/PCBM nanoparticles, the absorption spectrum of PCBM-doped nanoparticles of rra-P3HT was also recorded, which is shown as the dashed curve in the Figure 2a inset. The vibronic structure observed in the rr-P3HT nanoparticle spectrum is absent in the rra-P3HT nanoparticle absorption spectrum. The absorption maximum of rra-P3HT is red-shifted by 5 nm compared with that of the polymer dissolved in THF, as shown in the Supporting Information, where it adopts an extended conformation. In contrast, the absorption maximum for rr-P3HT is 30 nm to the red of the rra-P3HT absorption peak, which indicates a significant increase in the average chromophore length despite being subject to the same constraints of the nanoparticle structure.[35] This chromophore elongation is associated with planarization of the thiophene units, similar to that observed in thin films of rr-P3HT.[36,37]

Figure 2b shows that the fluorescence maximum of rr-P3HT is at 650 nm, which is red-shifted substantially by 55 nm relative to rra-P3HT nanoparticles, which is a further indication that a longer average conjugation length is supported by the highly ordered structure within rr-P3HT nanoparticles. The amplitudes of the vibronic progressions in the fluorescence spectrum of rr-P3HT nanoparticles, which are shown in Figure 2b, indicate the presence of H-aggregates.[38] The fluorescence intensity of rr-P3HT nanoparticles is quenched by the addition of PCBM, but the shape of the fluorescence spectrum remains unchanged. These results are consistent with efficient charge transfer, as quenching of P3HT fluorescence by PCBM requires charge transfer to occur considerably faster than the exciton recombination.[39] Even at a high PCBM doping level of 50 wt %, a portion of the fluorescence of P3HT remains unquenched which is attributable to P3HT excitons that are isolated from the PCBM interface. This result suggests that the formation of P3HT domains within rr-P3HT nanoparticles enables exciton recombination to occur before the exciton encounters any electron acceptor. The inset of Figure 2b shows the fluorescence of rr-P3HT and rra-P3HT as a function of PCBM doping level. Quenching of fluorescence is significantly more efficient for rra-P3HT than rr-P3HT, which suggests that rra-P3HT nanoparticles possess a more homogeneous PCBM distribution and therefore a shorter average distance from excitation to P3HT/PCBM interface.

The propensity for rr-P3HT to form large ordered semicrystalline domains has a considerable effect on the efficiency of charge transfer in P3HT/PCBM nanoparticles. Formation of these domains constrains the regions available to PCBM within a nanoparticle, causing it to aggregate. As a result, the available surface area of the P3HT/PCBM interface is limited relative to nanoparticles prepared with rra-P3HT, which is reflected by the fluorescence quenching data.

Femtosecond Transient Absorption Spectroscopy. Femtosecond transient absorption has been used routinely for investigating the formation of excited-state and charge-separated species in P3HT/PCBM films.[24,27,28,32,40] However, this work is the first transient absorption study on aqueous rr-P3HT nanoparticle suspensions containing PCBM. The transient absorption spectra of 0 and 50 wt % PCBM doped rr-P3HT nanoparticles at various delay times are shown in Figure 3. The pump wavelength of 500 nm is known to excite both the amorphous and semicrystalline domains of rr-P3HT aggregates.[25] For the undoped rr-P3HT nanoparticles, there is a broad excited-state absorption band centered around 1250 nm, as shown in Figure 3a. Previous studies on rr-P3HT films have shown that this absorption signal is attributable to polymer singlet excitons.[32]

Figure 3b shows that upon incorporation of PCBM into these nanoparticles there are fewer singlet excitons produced immediately following excitation. As the singlet exciton signal of the PCBM-doped nanoparticles diminishes, another excited-state absorption band emerges around 1000 nm and it persists

dx.doi.org/10.1021/jp308876z | J. Phys. Chem. B XXXX, XXX, XXX−XXX

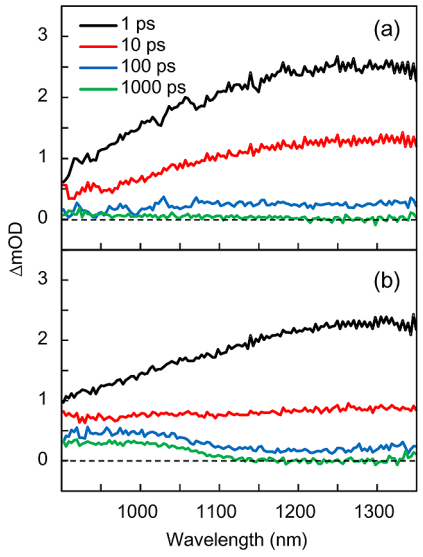

Figure 3. Transient absorption spectra of (a) undoped rr-P3HT nanoparticles and (b) rr-P3HT nanoparticles with 50 wt % PCBM at 1 ps (black), 10 ps (blue), 100 ps (red), and 1000 ps (green) after excitation.

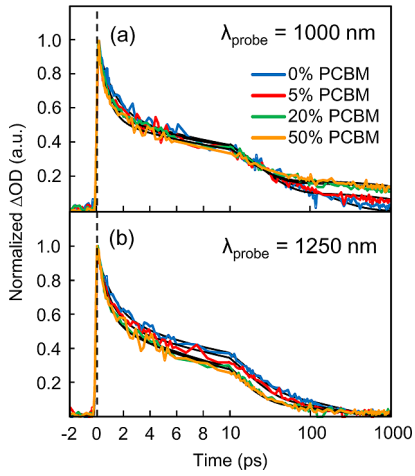

Figure 4. Kinetic traces at (a) 1000 nm and (b) 1250 nm for rr-P3HT nanoparticles doped with 0 (blue), 5 (red), 20 (green), and 50 (orange) wt % PCBM. The fitted curve for each sample is indicated by the corresponding solid black line. Note the change between a linear and a log scale at 10 ps.

for the entire measurable duration of these experiments. The long-lived absorption band at 1000 nm has been observed previously in film studies of rr-P3HT at higher pump intensities and has been assigned to formation of polymer polarons, i.e., hole polarons.[32] The results presented here are consistent with this assignment. First, as this absorption band is absent in undoped P3HT nanoparticles at the excitation intensities used in these experiments, it must be promoted by inclusion of the electron acceptor. Additionally, this excited-state absorption exhibits a decay on the order of several microseconds, much slower than that observed for polymer polaron pairs in the absence of PCBM.[28,41,42] Similarly, there is another excited-state absorption signal at 650 nm, which also becomes long-lived with the addition of PCBM, as shown in the Supporting Information. Both of these excited-state absorption signals that remain after 1 ns are attributable to the formation of free charges. It is important to note that the 1000 nm signal contains the dynamics of both singlet exciton decay and free charge formation, which will be discussed in more detail below.

Assignment of these various excited-state absorption signals can be further understood by examining the dynamics of each absorption band. Figure 4 shows the kinetic data for the excited-state absorptions at 1000 and 1250 nm for rr-P3HT nanoparticles doped with 0−50 wt % PCBM. All data were fitted with the minimum number of exponential decay terms required to adequately represent the data, as shown in the Supporting Information. As the limit of the delay stage used for these experiments was 2.5 ns, full recombination dynamics were not captured. As a result, processes with lifetimes overly long to be accurately determined were fitted as constant value offsets.

Figure 4a shows the 1000 nm excited-state absorption signals of P3HT nanoparticles from 5 to 50 wt % PCBM concentrations. These signals are well described by a triexponential function, as shown in the Supporting Information. The time constant of the first fitting component decreases as a function of PCBM doping level from 5 to 50 wt %, owing to the influence of the singlet exciton decay on the dynamics at this wavelength. The relative contribution of the third decay component increases with higher PCBM doping levels. The greater interfacial surface area at higher PCBM concentrations results in generation of more free charges that exhibit slow recombination dynamics.

The 1250 nm excited-state absorption signals of P3HT nanoparticles from 5 to 50 wt % PCBM concentrations are shown in Figure 4b. Assignment of this signal to singlet excitons is supported by the fitting parameters shown in the Supporting Information. The fastest decay component, which has a time constant of ∼1 ps, has an amplitude that increases proportionally with PCBM concentration, indicating the quenching of singlet excitons through charge transfer. As mentioned earlier, this singlet exciton signal decays substantially within 100 ps due to recombination, which confirms that no formation of free charges is observed at this wavelength. Furthermore, the power dependence on the singlet exciton recombination dynamics, which is presented in the Supporting Information, shows faster decay at higher excitation power, as would be expected for an increase in exciton−exciton annihilation.

It is interesting to compare the singlet exciton dynamics of undoped P3HT nanoparticles with that of P3HT films to offer insight into the effect of polymer conformation. The 1250 nm excited-state absorption signal of the undoped P3HT nanoparticles is well described by a triexponential function with time constants of 1.3, 16, and 200 ps, as shown in the Supporting Information. This multiexponential exciton decay contrasts with the single-exponential singlet exciton lifetime of annealed P3HT films.[27] Whereas the 200 ps decay component of the undoped P3HT nanoparticles corresponds to the singlet exciton lifetime,[27] the 1.3 and 16 ps decay components are related to other processes. First, the 1250 nm excited-state absorption signal exhibits an initial spectral shift within the first picosecond after excitation, indicating the presence of fast exciton migration. It is highly likely that the 1.3 ps decay component corresponds to exciton migration within the nanoparticles. A significant level of exciton migration is expected to occur because of the close proximity of chromophoric units in the compact structure of the nanoparticle. Second, recent studies have shown that torsional relaxation of P3HT occurs on a time scale of approximately 15

dx.doi.org/10.1021/jp308876z | J. Phys. Chem. B XXXX, XXX, XXX−XXX

ps.[43,44] In particular, torsional relaxation has been observed in aggregates of P3HT.[44] As a result, we attribute the 16 ps decay component in the excited-state absorption to torsional relaxation of P3HT nanoparticles. In contrast, torsional relaxation has a negligible role in the exciton dynamics in annealed films due to the presence of a highly ordered, crystalline phase. In short, the results suggest that exciton migration and torsional relaxation are involved in the initial dynamics of excitons in undoped P3HT nanoparticles.

Diffusion Model. The one-dimensional diffusion model of Kirkpatrick et al. was used to analyze the 1000 nm transient absorption signal, as shown in Figure 5.[27] Briefly, the model

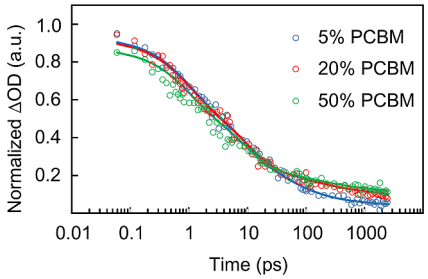

Figure 5. Decay of transient absorption signal at 1000 nm for 5 (black), 10 (blue), 20 (red), and 50 (green) wt % PCBM. The corresponding fits from the exciton diffusion model are shown as solid lines.

describes the competition between charge transfer and exciton decay for a P3HT domain bounded by PCBM. Excitons within P3HT decay according to the excited-state lifetime (τ_r). If excitons reach the P3HT/PCBM interface during this time, they form a charge transfer state. In this model, the exciton population $\xi(t)$ per absorbed photon varies with time according to

$$\xi(t) = \sum_{n_{odd}} \frac{8}{\pi^2 n^2} \exp\left[-\left(\frac{\pi^2 n^2 D}{L^2} + \frac{1}{\tau_r}\right)t\right] \quad (1)$$

where L is the P3HT domain size and D is the exciton diffusion constant in P3HT, which is related to the exciton diffusion length L_{ex} by $L_{ex} = (D\tau_r)^{1/2}$. To account for the multi-exponential and considerably faster exciton decay in nanoparticles compared with films, the model was altered to include two exciton recombination time constants, τ_{r_1} and τ_{r_2}, giving the following modified equation for the exciton population:

$$\xi(t) = a_1 \sum_{n_{odd}} \frac{8}{\pi^2 n^2} \exp\left[-\left(\frac{\pi^2 n^2 D}{L^2} + \frac{1}{\tau_{r_1}}\right)t\right] + a_2 \sum_{n_{odd}} \frac{8}{\pi^2 n^2} \exp\left[-\left(\frac{\pi^2 n^2 D}{L^2} + \frac{1}{\tau_{r_2}}\right)t\right] \quad (2)$$

where the relative amplitudes a_1 and a_2 were determined from the pure P3HT nanoparticle decay and were held constant for all concentrations of PCBM. The equations in the model for the polaron population and transient absorbance were modified accordingly to account for the additional relaxation time. The instantaneous rate of charge generation depends on the exciton population that can migrate successfully to the interface. Once the charge transfer state is formed it can undergo either geminate or bimolecular recombination. It has been proposed that geminate recombination can potentially follow either exponential or power law decay at short times depending on the level of disorder in P3HT and the concentration of the electron acceptor.[27] In both cases, geminate recombination is followed by bimolecular recombination, which is represented by a power law decay. For exponential geminate recombination the polaron population $p(t)$ at time t per exciton dissociated at time zero in the model is given by

$$p(t) = \exp\left(\frac{-\tau_b}{\tau_g}\right) \exp\left(\frac{{\tau_b}^2}{t\tau_g + \tau_b\tau_g}\right)\left(1 + \frac{t}{\tau_b}\right)^{-\alpha} \quad (3)$$

This exponential geminate recombination model gave the best description of our data and was used to fit all transient absorption decays presented here. In this case, the proportion of charges that undergo bimolecular recombination, which is given by the first term in eq 3, depends on the time constant of geminate recombination (τ_g), and the time constant for charge separation (τ_b). Those charges that overcome the Coulombic binding energy successfully to form free charges will recombine according to the power law decay term with an exponent of α. Convolving the rate of charge generation with the temporal evolution of the generated charges pairs gives the total charge population. Finally, the transient absorption signal can be calculated from the exciton decay, total charge population, and the relative extinction coefficient (ε_{rel}) of excitons and charges at 1000 nm.

The transient absorption data at 1000 nm, shown in Figure 5, were fitted with this model. In the analysis, the τ_{r_1} and τ_{r_2} values were fixed at 1 and 15 ps, respectively, for all PCBM concentrations. These values are consistent with the first two decay time constants of the exciton dynamics, which are inferred from the transient absorption signal at 1250 nm. The value of τ_b was fixed at 100 ps, which is the same as that reported by Kirkpatrick et al.,[27] because the charge separation process is expected to be the same in P3HT films and nanoparticles. A representative α value of 0.11 was determined using the recombination dynamics of free charges in P3HT nanoparticles at various PCBM concentrations. The relative extinction coefficient of exciton and free charges at 1000 nm were taken to be unity and 0.8, respectively, and were held constant across all PCBM concentrations.[27] The average P3HT domain length and geminate recombination time constant were obtained by fitting each transient absorption decay to the model. The best fit parameters are shown in Table 1.

Table 1. Fitted Parameters Determined from the Charge Transfer Model

PCBM wt %	L (nm)	τ_g (ps)
5	4.8 ± 2.0	67 ± 25
20	5.6 ± 1.5	170 ± 80
50	5.6 ± 1.5	260 ± 190

The average P3HT domain size is consistent across the range of PCBM concentrations studied here given the degree of uncertainty present in the data. Our results show good agreement with the size of P3HT domains in annealed films with high PCBM concentrations, implying that the morphology of the nanoparticles is similar to that of films annealed at elevated temperatures. This agreement is unexpected because the formation of P3HT nanoparticles occurs at room temperature. However, it is important to stress that exclusion

dx.doi.org/10.1021/jp308876z | J. Phys. Chem. B XXXX, XXX, XXX−XXX

of water, a poor solvent for P3HT, is accompanied by the collapse of P3HT chains in the formation of nanoparticles. Therefore, our results suggest that exclusion of water from P3HT chains has an effect on morphology similar to that of annealing the chains thermally. In addition, it is instructive to compare the P3HT domain lengths to the diameters of nanoparticles at various PCBM concentrations, which are given in the Supporting Information, to understand the relationship between nanoparticles and annealed films. The P3HT/PCBM nanoparticles are only approximately 6−11 times larger than the domain sizes and are therefore expected to behave differently from bulk materials due to a significant surface-to-volume ratio. It is surprising that confined and bulk materials prepared under such different conditions exhibit similar domain sizes.

Additionally, the size of PCBM aggregates for each PCBM concentration was calculated by assuming a homogeneous distribution of spherical and equally sized PCBM aggregates. Although several reports have shown PCBM forms needle-like aggregates in annealed films,[30,45] the fitting of our spectroscopic data to the diffusion model yields only a single characteristic spatial dimension for the P3HT domains and hence only a single characteristic length for the PCBM domains can be inferred from this analysis. Although calculating this length requires that an aggregate shape described by a single length scale such as a sphere or cube be assumed, the resulting length should be regarded as the characteristic size of the domains rather than the diameter of actual spherical PCBM aggregates. For this calculation, the volume fractions of PCBM were determined from the PCBM doping ratio and the densities of crystalline P3HT and crystalline PCBM, which have values of 1.12 and 1.67 g/cm^3, respectively.[46,47] The resulting diameters of PCBM aggregates were found to be 3.2, 10.4, and 60.5 nm for 5, 20, and 50 wt % PCBM, respectively. The diameter of the aggregate in the 50 wt % PCBM sample is unreliable as the assumption of equally sized and homogeneously distributed PCBM aggregates is inadequate when the PCBM content becomes a large fraction of the total nanoparticle mass.

As mentioned above, the power-law decay observed in composite P3HT/PCBM nanoparticles has an α value of 0.11 and occurs more rapidly than that observed for films where α = 0.05. The magnitude of the power-law decay exponent α indicates the quantity of deep trap states in P3HT films, with higher exponents indicating fewer trap states.[23] Our result suggests that fewer trap states are formed during nanoparticle preparation than in P3HT films. It is well understood that deep traps for charges are facilitated by the presence of large domains of high crystallinity because the grain boundaries around these domains act to trap charges.[48] Therefore, the presence of fewer deep trap states in the P3HT/PCBM nanoparticles than in films suggests that there are fewer grain boundaries around the crystalline domains than those found in annealed films.

From the exciton diffusion model, we were also able to determine the geminate recombination time constant and the proportion of charges that recombine through geminate and bimolecular recombination.[27] The geminate recombination time constant increases from 67 to 260 ps as the PCBM concentration increases from 5 to 50 wt % PCBM. These τ_g values indicate that the proportions of charges that undergo bimolecular recombination are 22%, 56%, and 68% for 5, 20, and 50 wt % PCBM, respectively, with a fixed τ_b value of 100 ps. At PCBM concentrations of 10 wt % and below, charges recombine predominantly by geminate recombination, whereas at higher concentrations bimolecular recombination is the primary mechanism. The likely cause for the increase in the geminate recombination time constant as a function of PCBM concentration is the formation of larger PCBM aggregates, as demonstrated by the estimates mentioned earlier. Larger aggregates of PCBM allow effective migration of charge pairs, thereby reducing the probability of geminate recombination. Considering the observed trend in geminate recombination time constant, it is likely that increasing the PCBM concentration causes the aggregates of PCBM in the nanoparticle to become larger rather than forming a greater number of relatively small aggregates, in agreement with the PCBM aggregate sizes calculated from the model.

CONCLUSION

We have presented steady-state and transient optical spectroscopic data of charge transfer in P3HT/PCBM composite nanoparticles. Steady-state absorption and fluorescence quenching data show vastly contrasting behavior between nanoparticles prepared with rr-P3HT and rra-P3HT. The rr-P3HT/PCBM nanoparticles contain extended semicrystalline domains of P3HT that confine PCBM to aggregates, whereas amorphous nanoparticles of rra-P3HT exhibit a more homogeneous distribution of PCBM. Excited-state and charge-transfer species in rr-P3HT/PCBM composite nanoparticles were identified using visible pump and visible/near-infrared probe femtosecond transient absorption spectroscopy. The signals at 1000 and 1250 nm were assigned to free charges and singlet excitons, respectively, which show good agreement with previous studies on films. The 1000 nm signal, which includes contributions from both singlet exciton decay and free charge formation, was fit to a one-dimensional diffusion model to determine the size of the P3HT domains and the rate of geminate recombination. The size of P3HT domains decreases with increased PCBM concentration in accordance with the quenching of the excited-state lifetime by competitive charge transfer to PCBM. Geminate recombination of charges is the dominant mechanism at low electron acceptor concentrations, whereas at high PCBM concentrations bimolecular recombination is favored. The increase in bimolecular recombination with PCBM concentration is likely to be caused by the formation of larger PCBM aggregates rather than a greater number small aggregates, as in this case charges are less likely to be confined by the size of the PCBM aggregates. The results presented here are in good agreement with studies on rr-P3HT/PCBM films, which confirms that these composite nanoparticles are suitable model systems for polymer bulk-heterojunction devices.

ASSOCIATED CONTENT

Supporting Information

Absorption spectra of rr-P3HT and rra-P3HT in THF, fluorescence spectra of PCBM doped rra-P3HT nanoparticles, transient absorption spectra in the visible range, tables containing fitting parameters for the kinetics of excited-state absorption signals, power dependence of the 1250-nm single exciton signal, and particle size characterization by AFM. This material is available free of charge via the Internet at http://pubs.acs.org.

AUTHOR INFORMATION

Corresponding Author

*E-mail: tak.kee@adelaide.edu.au.

Notes

The authors declare no competing financial interest.

■ ACKNOWLEDGMENTS

This work was supported by a research grant from the Australian Research Council (LE0989747).

■ REFERENCES

(1) Wu, C. F.; Szymanski, C.; McNeill, J. Preparation and Encapsulation of Highly Fluorescent Conjugated Polymer Nanoparticles. *Langmuir* **2006**, *22*, 2956−2960.
(2) Wu, C.; Szymanski, C.; Cain, Z.; McNeill, J. Conjugated Polymer Dots for Multiphoton Fluorescence Imaging. *J. Am. Chem. Soc.* **2007**, *129*, 12904−12905.
(3) Wu, C.; Schneider, T.; Zeigler, M.; Yu, J.; Schiro, P. G.; Burnham, D. R.; McNeill, J. D.; Chiu, D. T. Bioconjugation of Ultrabright Semiconducting Polymer Dots for Specific Cellular Targeting. *J. Am. Chem. Soc.* **2010**, *132*, 15410−15417.
(4) Wu, C.; Bull, B.; Szymanski, C.; Christensen, K.; McNeill, J. Multicolor Conjugated Polymer Dots for Biological Fluorescence Imaging. *ACS Nano* **2008**, *2*, 2415−2423.
(5) Wu, C.; McNeill, J. Swelling-Controlled Polymer Phase and Fluorescence Properties of Polyfluorene Nanoparticles. *Langmuir* **2008**, *24*, 5855−5861.
(6) Ye, F.; Wu, C.; Jin, Y.; Chan, Y.-H.; Zhang, X.; Chiu, D. T. Ratiometric Temperature Sensing with Semiconducting Polymer Dots. *J. Am. Chem. Soc.* **2011**, *133*, 8146−8149.
(7) Jin, Y.; Ye, F.; Zeigler, M.; Wu, C.; Chiu, D. T. Near-Infrared Fluorescent Dye-Doped Semiconducting Polymer Dots. *ACS Nano* **2011**, *5*, 1468−1475.
(8) Chan, Y.-H.; Wu, C.; Ye, F.; Jin, Y.; Smith, P. B.; Chiu, D. T. Development of Ultrabright Semiconducting Polymer Dots for Ratiometric pH Sensing. *Anal. Chem.* **2011**, *83*, 1448−1455.
(9) Davis, C. M.; Childress, E. S.; Harbron, E. J. Ensemble and Single-Particle Fluorescence Photomodulation in Diarylethene-Doped Conjugated Polymer Nanoparticles. *J. Phys. Chem. C* **2011**, *115*, 19065−19073.
(10) Childress, E. S.; Roberts, C. A.; Sherwood, D. Y.; LeGuyader, C. L. M.; Harbron, E. J. Ratiometric Fluorescence Detection of Mercury Ions in Water by Conjugated Polymer Nanoparticles. *Anal. Chem.* **2012**, *84*, 1235−1239.
(11) Wu, C.; Bull, B.; Christensen, K.; McNeill, J. Ratiometric Single-Nanoparticle Oxygen Sensors for Biological Imaging. *Angew. Chem., Int. Ed.* **2009**, *48*, 2741−2745.
(12) Tenery, D.; Gesquiere, A. J. Effect of PCBM Concentration on Photoluminescence Properties of Composite MEH-PPV/PCBM Nanoparticles Investigated by a Franck-Condon Analysis of Single-Particle Emission Spectra. *ChemPhysChem* **2009**, *10*, 2449−2457.
(13) Hu, Z.; Gesquiere, A. J. PCBM Concentration Dependent Morphology of P3HT in Composite P3HT/PCBM Nanoparticles. *Chem. Phys. Lett.* **2009**, *476*, 51−55.
(14) Hu, Z.; Gesquiere, A. J. Charge Trapping and Storage by Composite P3HT/PC60BM Nanoparticles Investigated by Fluorescence-Voltage/Single Particle Spectroscopy. *J. Am. Chem. Soc.* **2011**, *133*, 20850−20856.
(15) Hu, Z.; Tenery, D.; Bonner, M. S.; Gesquiere, A. J. Correlation Between Spectroscopic and Morphological Properties of Composite P3HT/PCBM Nanoparticles Studied by Single Particle Spectroscopy. *J. Lumin.* **2010**, *130*, 771−780.
(16) Minh Trung, D.; Hirsch, L.; Wantz, G. P3HT:PCBM, Best Seller in Polymer Photovoltaic Research. *Adv. Mater.* **2011**, *23*, 3597−3602.
(17) Lee, S.-H.; Kim, D.-H.; Kim, J.-H.; Lee, G.-S.; Park, J.-G. Effect of Metal-Reflection and Surface-Roughness Properties on Power-Conversion Efficiency for Polymer Photovoltaic Cells. *J. Phys. Chem. C* **2009**, *113*, 21915−21920.
(18) Lee, S.-H.; Kim, J.-H.; Shim, T.-H.; Park, J.-G. Effect of Interface Thickness on Power Conversion Efficiency of Polymer Photovoltaic Cells. *Electron. Mater. Lett.* **2009**, *5*, 47−50.
(19) Sondergaard, R.; Helgesen, M.; Jorgensen, M.; Krebs, F. C. Fabrication of Polymer Solar Cells Using Aqueous Processing for All Layers Including the Metal Back Electrode. *Adv. Energy Mater.* **2011**, *1*, 68−71.
(20) Stapleton, A.; Vaughan, B.; Xue, B.; Sesa, E.; Burke, K.; Zhou, X.; Bryant, G.; Werzer, O.; Nelson, A.; Kilcoyne, A. L. D.; et al. A Multilayered Approach to Polyfluorene Water-Based Organic Photovoltaics. *Sol. Energy Mater. Sol. Cells* **2012**, *102*, 114−124.
(21) Tenery, D.; Worden, J. G.; Hu, Z.; Gesquiere, A. J. Single Particle Spectroscopy on Composite MEH-PPV/PCBM Nanoparticles. *J. Lumin.* **2009**, *129*, 423−429.
(22) Tenery, D.; Gesquiere, A. J. Interplay Between Fluorescence and Morphology in Composite MEH-PPV/PCBM Nanoparticles Studied at the Single Particle Level. *Chem. Phys.* **2009**, *365*, 138−143.
(23) Clarke, T. M.; Ballantyne, A. M.; Nelson, J.; Bradley, D. D. C.; Durrant, J. R. Free Energy Control of Charge Photogeneration in Polythiophene/Fullerene Solar Cells: The Influence of Thermal Annealing on P3HT/PCBM Blends. *Adv. Funct. Mater.* **2008**, *18*, 4029−4035.
(24) Guo, J.; Ohkita, H.; Benten, H.; Ito, S. Charge Generation and Recombination Dynamics in Poly(3-hexylthiophene)/Fullerene Blend Films with Different Regioregularities and Morphologies. *J. Am. Chem. Soc.* **2010**, *132*, 6154−6164.
(25) Honda, S.; Yokoya, S.; Ohkita, H.; Benten, H.; Ito, S. Light-Harvesting Mechanism in Polymer/Fullerene/Dye Ternary Blends Studied by Transient Absorption Spectroscopy. *J. Phys. Chem. C* **2011**, *115*, 11306−11317.
(26) Howard, I. A.; Mauer, R.; Meister, M.; Laquai, F. Effect of Morphology on Ultrafast Free Carrier Generation in Polythiophene:-Fullerene Organic Solar Cells. *J. Am. Chem. Soc.* **2010**, *132*, 14866−14876.
(27) Kirkpatrick, J.; Keivanidis, P. E.; Bruno, A.; Ma, F.; Haque, S. A.; Yarstev, A.; Sundstrom, V.; Nelson, J. Ultrafast Transient Optical Studies of Charge Pair Generation and Recombination in Poly-3-Hexylthiophene(P3ht):[6,6]Phenyl C61 Butyric Methyl Acid Ester (PCBM) Blend Films. *J. Phys. Chem. B* **2011**, *115*, 15174−15180.
(28) Ohkita, H.; Cook, S.; Astuti, Y.; Duffy, W.; Tierney, S.; Zhang, W.; Heeney, M.; McCulloch, I.; Nelson, J.; Bradley, D. D. C.; et al. Charge Carrier Formation in Polythiophene/Fullerene Blend Films Studied by Transient Absorption Spectroscopy. *J. Am. Chem. Soc.* **2008**, *130*, 3030−3042.
(29) Singh, S.; Pandit, B.; Basel, T. P.; Li, S.; Laird, D.; Vardeny, Z. V. Two-Step Charge Photogeneration Dynamics in Polymer/Fullerene Blends for Photovoltaic Applications. *Phys. Rev. B* **2012**, *85*, 205206.
(30) Wong, C. T. O.; Lo, S. S.; Huang, L. Ultrafast Spatial Imaging of Charge Dynamics in Heterogeneous Polymer Blends. *J. Phys. Chem. Lett.* **2012**, *3*, 879−884.
(31) Zhang, W.; Hu, R.; Li, D.; Huo, M.-M.; Ai, X.-C.; Zhang, J.-P. Primary Dynamics of Exciton and Charge Photogeneration in Solvent Vapor Annealed P3HT/PCBM Films. *J. Phys. Chem. C* **2012**, *116*, 4298−4310.
(32) Guo, J.; Ohkita, H.; Benten, H.; Ito, S. Near-IR Femtosecond Transient Absorption Spectroscopy of Ultrafast Polaron and Triplet Exciton Formation in Polythiophene Films with Different Regioregularities. *J. Am. Chem. Soc.* **2009**, *131*, 16869−16880.
(33) Clafton, S. N.; Beattie, D. A.; Mierczynska-Vasilev, A.; Acres, R. G.; Morgan, A. C.; Kee, T. W. Chemical Defects in the Highly Fluorescent Conjugated Polymer Dots. *Langmuir* **2010**, *26*, 17785−17789.
(34) Mihailetchi, V. D.; Xie, H.; de, B. B.; Koster, L. J. A.; Blom, P. W. M. Charge Transport and Photocurrent Generation in Poly(3-hexylthiophene):Methanofullerene Bulk-Heterojunction Solar Cells. *Adv. Funct. Mater.* **2006**, *16*, 699−708.
(35) Scharsich, C.; Lohwasser, R. H.; Sommer, M.; Asawapirom, U.; Scherf, U.; Thelakkat, M.; Neher, D.; Koehler, A. Control of Aggregate Formation in Poly(3-hexylthiophene) by Solvent, Molecular Weight,

and Synthetic Method. *J. Polym. Sci., Part B: Polym. Phys.* **2012**, *50*, 442−453.
(36) Kline, R. J.; McGehee, M. D.; Kadnikova, E. N.; Liu, J.; Fréchet, J. M. J.; Toney, M. F. Dependence of Regioregular Poly(3-hexylthiophene) Film Morphology and Field-Effect Mobility on Molecular Weight. *Macromolecules* **2005**, *38*, 3312−3319.
(37) Erb, T.; Zhokhavets, U.; Gobsch, G.; Raleva, S.; Stühn, B.; Schilinsky, P.; Waldauf, C.; Brabec, C. J. Correlation Between Structural and Optical Properties of Composite Polymer/Fullerene Films for Organic Solar Cells. *Adv. Funct. Mater.* **2005**, *15*, 1193−1196.
(38) Spano, F. C. The Spectral Signatures of Frenkel Polarons in H- and J-Aggregates. *Acc. Chem. Res.* **2010**, *43*, 429−439.
(39) Piris, J.; Dykstra, T. E.; Bakulin, A. A.; van Loosdrecht, P. H. M.; Knulst, W.; Trinh, M. T.; Schins, J. M.; Siebbeles, L. D. A. Photogeneration and Ultrafast Dynamics of Excitons and Charges in P3HT/PCBM Blends. *J. Phys. Chem. C* **2009**, *113*, 14500−14506.
(40) Hwang, I.-W.; Moses, D.; Heeger, A. J. Photoinduced Carrier Generation in P3HT/PCBM Bulk Heterojunction Materials. *J. Phys. Chem. C* **2008**, *112*, 4350−4354.
(41) Nogueira, A. F.; Montanari, I.; Nelson, J.; Durrant, J. R.; Winder, C.; Sariciftci, N. S. Charge Recombination in Conjugated Polymer/Fullerene Blended Films Studied by Transient Absorption Spectroscopy. *J. Phys. Chem. B* **2003**, *107*, 1567−1573.
(42) Nelson, J. Diffusion-Limited Recombination in Polymer-Fullerene Blends and its Influence on Photocurrent Collection. *Phys. Rev. B* **2003**, *67*.
(43) Xie, Y.; Li, Y.; Xiao, L.; Qiao, Q.; Dhakal, R.; Zhang, Z.; Gong, Q.; Galipeau, D.; Yan, X. Femtosecond Time-Resolved Fluorescence Study of P3HT/PCBM Blend Films. *J. Phys. Chem. C* **2010**, *114*, 14590−14600.
(44) Parkinson, P.; Müller, C.; Stingelin, N.; Johnston, M. B.; Herz, L. M. Role of Ultrafast Torsional Relaxation in the Emission from Polythiophene Aggregates. *J. Phys. Chem. Lett.* **2010**, *1*, 2788−2792.
(45) Swinnen, A.; Haeldermans, I.; vande Ven, M.; D'Haen, J.; Vanhoyland, G.; Aresu, S.; D'Olieslaeger, M.; Manca, J. Tuning the Dimensions of C60-Based Needlelike Crystals in Blended Thin Films. *Adv. Funct. Mater.* **2006**, *16*, 760−765.
(46) Prosa, T. J.; Winokur, M. J.; Moulton, J.; Smith, P.; Heeger, A. J. X-ray Structural Studies of Poly(3-alkylthiophene) - an Example of an Inverse Comb. *Macromolecules* **1992**, *25*, 4364−4372.
(47) Rispens, M. T.; Meetsma, A.; Rittberger, R.; Brabec, C. J.; Sariciftci, N. S.; Hummelen, J. C. Influence of the Solvent on the Crystal Structure of PCBM and the Efficiency of MDMO-PPV: PCBM 'Plastic' Solar Cells. *Chem. Commun.* **2003**, 2116−2118.
(48) Kaake, L. G.; Barbara, P. F.; Zhu, X. Y. Intrinsic Charge Trapping in Organic and Polymeric Semiconductors: A Physical Chemistry Perspective. *J. Phys. Chem. Lett.* **2010**, *1*, 628−635.